A Land-cover Driven Approach for Fitting Satellite Image Time Series in a Change Detection Context

Yady Tatiana Solano-Correa[a], Khatereh Meshkini[a,b], Francesca Bovolo*[a], Lorenzo Bruzzone[b]
[a]Center for Information and Communication Technology, Fondazione Bruno Kessler, via Sommarive, 18 I-38123, Povo, Trento, Italy; [b]Department of Engineering and Computer Science, University of Trento, via Sommarive, 5 I-38123, Povo, Trento, Italy

ABSTRACT

Thanks to the freely availability of several Satellite Image Time Series (SITS) covering the Earth, it is now possible to monitor and analyse Land Covers (LC) and Land Cover Changes (LCC) on a yearly or even longer time span. Such applications are relevant in the context of Climate Change (CC), where consequences of the changes can only be seen on long term. Nevertheless, SITS suffer from atmospheric condition related problems (when talking about passive sensors) that reduce the temporal resolution of images in SITS. Several methods have been proposed in literature to mitigate these problems, and are placed under gap filling or SITS fitting methods. Such methods generally work with a single feature, being it a radiometric index or a spectral band. The use of multiple features is limited to specific single LC class or satellite sensor, limiting its usage in LCC and CC. Thus, in this paper, we propose an approach that is automatic, and both LC and feature independent. Here we propose the use of Normalized Difference Indices (NDI), with combination of all available spectral bands. The proposed approach uses a dropout upper-envelope strategy to reconstruct SITS trends, based on a set of rules, and guarantees a smoother closer trend to that of the original data. The proposed approach has been applied over two regions (Amazonia and Saudi Arabia) in the period 2013-2017, and has been compared to other fitting methods: Cubic Splines and Univariate Splines. It has been further evaluated by detecting LCC with long SITS methods such as Breaks For Additive Seasonal and Trend (BFAST). The preliminary results are promising demonstrating the robustness of the approach across different LCs and across different features.

Keywords: Land Cover Change, Fitting methods, Satellite Image Time Series, Normalized Difference Index, Land Cover

1. INTRODUCTION

Climate Change (CC) can be measured while studying its effects/impacts on Land Covers (LC). In this context, the analysis of persistent (decades or longer) Land Cover Changes (LCC) becomes a relevant indicator. CC may affect both water and carbon cycles when transitioning from one land cover to another occurs or when the intrinsic characteristics of a land cover type are altered. These factors are considered by the climate modelling community to properly model CC at a local or global scale, according to the spatial resolution of Earth Observation data. Thanks to the latest advances in technology, an increasing number of Satellite Image Time Series (SITS) for Earth monitoring is available. They provide a better trade off in terms of spatial/spectral/temporal resolution with respect to previous generation SITS and thus novel possibilities to studying LCC and its impacts in CC.

In order to achieve a better Change Detection (CD) in long SITS, the ideal would be to have continuous and/or regular SITS over time[1]. Nevertheless, the use of SITS acquired by optical passive sensors is limited by atmospheric conditions and other radiometric effects that reduce the data quality and thus the capability for performing LCC detection. Numerous efforts have been made[2–4] to develop methods able to properly fit/reconstruct multispectral reflectance and vegetation indices SITS for different LC. Nevertheless, such methods mainly compare vegetative profiles (Normalized Difference Vegetation Index (NDVI) or Enhanced Vegetation Index (EVI)) between inner class temporal signatures. The behaviors are modelled, taking into account vegetation cycles and cycling harmonics models[5–7]. As an example of this, Bradley *et al.*[2] proposed a 6th order annual harmonics model to create average annual phenology with a high order Spline-based fitting method. A 12 year SITS of weekly NDVI data from AVHRR satellite was used to estimate the onset of

*bovolo@fbk.eu phone: +39-0461-314503;

greenness. Atkinson *et al.*[3], used a combination of four fitting methods (Fourier asymmetric, Gaussian, Double Logistic and Whittaker filter) in order to smooth 8 days MERIS Terrestrial Chlorophyll Index (MTCI) data from 2003-2007. These data were used to determine onset of greenness and end of senescence for several types of natural vegetation covers. The usage of those strategies do not fit the case of multiple class trends (including non-vegetative classes) and fails in the presence of abrupt changes or number of cycles different from the pre-established values. The development of a strategy to automatically reconstruct the temporal signature of independent features and classes, and for different applications is needed.

Several other methods exist in literature that combine SITS fitting methods with CD ones in order to produce yearly change maps[8–10]. Such methods suffer from the same problem of rather focusing on a single application or assuming cyclic information. Zhu and Woodcock[10] proposed a method to perform continuous change detection and classification of intra-annual, inter-annual and abrupt changes, together with the generation of a LC map. To achieve this goal, they produced a time series model with seasonality, trend and breaks components. The model coefficients were estimated by the Ordinary Least Squares fitting method and based on only clear sky Landsat images (which reduces the possible amount of information) and only bands 2 and 5 of the sensor, reducing the spectral information and thus the change detection capabilities. Hermosilla *et al.*[9], made use of an annual Based Available Pixel (BAP) image composites and break point strategy to detect disturbances over forest based on a Normalized Burn Ratio (NBR) feature. BAPs work at pixel level and thus consider all possible cloud free pixels in the SITS, without penalizing the whole image.

Here we present a SITS fitting approach for multispectral data acquired at high spatial resolution (i.e., Landsat and Sentinel-2 like). The proposed approach can be LC driven, thus assuming the availability of a LC map. The method is fully automatic and can be applied to any type of multidimensional feature space and any type of LC. It works at single pixel level, thus exploiting all possible cloud free pixels in a SITS, and can possibly detect any type of abrupt change.

The paper is organized into five sections. The next section introduces the proposed approach to fitting SITS in the context of LCC. Section 3 describes the different study areas considered in the paper. Section 4 presents the results and discussion of the different application examples. Finally, section 5 draws the conclusions and provides future developments.

2. PROPOSED APPROACH TO FITTING SATELLITE IMAGE TIME SERIES IN A CHANGE DETECTION CONTEXT

Properly detecting land cover changes in long SITS allows for a better understanding of CC drivers, and is highly dependent of continuous data in time. Nevertheless, literature lacks of methods being general enough to work in the same way for different types of LCs. Because of this, we propose an automatic and robust method to perform reliable SITS fitting that is class and feature independent. Figure 1 depicts de general block scheme of the proposed approach to fitting SITS in a land cover CD context. The proposed approach is based on four steps: (i) automatic retrieval and filtering of data, (ii) feature extraction, (iii) time series regularization and; (iv) Land Cover Change Detection (LCCD). The approach is general enough to be applied in the same way to any High Resolution (HR) sensor. In the first step, the automatic retrieval is achieved thanks to the use of Google Earth Engine (GEE)[11] platform and the filtering refers to cloudy pixels in the SITS. The second step performs the feature extraction based on Normalized Difference Indices (NDI). The third step applies the proposed SITS fitting that can be LC-driven, if a LC map is available, and finally step four builds a CD HR map, according to the years in which a change has occurred. This final CD HR map can be used by climatologist in order to further understand possible CC drivers.

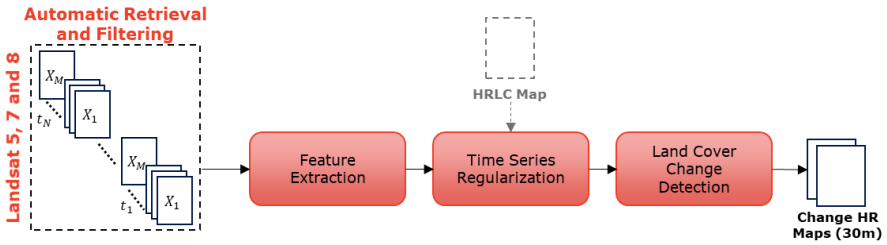

Figure 1. Block Scheme for the proposed approach for fitting SITS in a change detection context.

Let $SITS = \{X_1, X_2, \dots, X_N\}$ be a pre-processed Satellite Image Time Series acquired over the same geographical area in the period $[t_1, t_N]$. Assume the SITS have non-uniform time sampling, and each $X_n (n = 1, \dots, N)$ includes P pixels. Given an image X_n, each pixel value represents the surface reflectance at a given spatial position and temporal instant t_n. Let

$SITS_p$ (with $1 < p < P$) be the temporal signature of a pixel P in the interval $[t_1, t_N]$. Let $B = \{b_1, b_2, \dots, b_K\}$ be the set of bands that compose images X_n and K the total number of bands. The temporal signature of each pixel is strictly related to the LC and Land Use (LU).

2.1 Automatic retrieval and filtering of SITS

Nowadays, there exist several options to download satellite data. Nevertheless, this process has several implications and problems from cloud platforms to local storage limitations, especially when considering long SITS. In order to mitigate such problems, a good alternative is to use GEE[11], a cloud platform that not only contains free satellite datasets, but also allows the processing of big amounts of data at no cost and in a fast manner. For this paper, we make use of GEE to download the data, and exploit available cloud masks (from GEE data collections) in order to filter out cloudy pixels from the SITS that could introduce noise or false changes over time. A cloud mask condition is imposed in order to avoid adding cloudy pixels in any $SITS_p$. Since cloudy pixels are not located in the same place over the SITS, this condition is applied at single pixel level only, avoiding the loss of reliable information in surrounding pixels and thus maximizing the amount of usable data in time and space. As a result, $SITS_p$ are irregular w.r.t. the original temporal resolution of the HR sensor, but also among each other.

2.2 Feature Extraction

The choice of a suitable Feature Space (FS) is one of the fundamental elements to distinguish the spectral trends of different sets of LC changes. All possible couples of the available original sensor bands are considered to compute a set of Normalized Difference Indices ($NDI_f, f = (1, \dots, F)$ – see equation (1)). This stage transforms the B-dimensional FS into a F-dimensional FS (see equation (2)). The employment of NDIs, reduces the undesirable oscillations that affect the spectral bands. The normalized difference ratio between different bands is selected as the best feature given its high use in the analysis between different classes. Examples of this are the several indices available in literature and frequently use in classification or single class monitoring/CD. The NDI values (included in the $[-1, 1]$ interval), are also suitable to perform more general and reliable comparisons in successive steps.

$$NDI_f = \frac{B_i - B_j}{B_i + B_j}, f = (1, \dots, F) \quad (1)$$

where B_i and B_j belong to B, the set of bands available in a sensor, and i and $j \in [1,2, \dots, K]$.

$$F = \frac{1}{2}(K - 1) \times K \quad (2)$$

2.3 Time Series Regularization

At this stage, the temporal signature is a raw signal characterized by non-equally distributed temporal sampling and non-continuous trend, also affected by noisy oscillation not corrected in the pre-processing step. Irregular temporal data limits the accuracy of the change detection itself. This is because estimation methods (SITS-CD ones) assume equally spaced regular data in the time domain. The time series regularization stage allows generating a sequence of values, denser than the source signal. The temporal signature is expected to be a truthful, smooth and continuous behavior. To this end, preliminary symmetrical and uniformly sampled NDI-SITS need to be generated. Usually this is achieved by a linear combination of nearby values in the SITS in a window[12]. We propose an alternative novel approach, that is LC and feature independent, where a smoothed SITS is simulated generating daily acquisitions by data augmentation of the NDI-SITS upper-envelope with a withdrawn strategy.

The SITS regularization is based on two steps: i) for each pixel in the image extract the NDI-SITS, ii) perform NDI data-SITS augmentation by upper envelope and dropout strategy (a piecewise cubic interpolation is used here). In the case of complex LC classes, that show strong variabilities over space and time due to intrinsic seasonality and the large amount of species around the world, like vegetation type (i.e., grass, shrubs, forest and crops), a third step can be optionally added that performs adaptive non-parametric regression of NDI-SITS by considering a General Regression Neural Network (GRNN). This step is only applied if a LC map is available. Further details on the augmentation by upper envelope strategy are illustrated as follows[13,14]:

- Define a NDI-SITS set (NDI_{tr}), corresponding to a year (365 days), plus the two previous and two later months of data;

- For each NDI_{tr}, select the samples that are above a given threshold (defined by trial and error as NDI = 0.4). This threshold identifies when a given $SITS_p$ experiences a significant variability over time;
- Calculate the local maxima (as the points with zero first derivative and negative second derivative) of the selected samples and withdraw the remaining ones (from NDI_{tr}). This leads to the upper envelope of the data;
- Use the samples below the threshold and the local maxima from previous step for data imputation by means of a Piecewise Cubic Hermite Interpolating Polynomial (PCHIP). The selection of PCHIP over other interpolation methods is justified by its characteristic to preserve the shape of the data and respect monotonicity. The combination of these samples is defined as the upper-envelope set;
- Subtract the imputed data from NDI_{tr}. Reinsert the withdrawn samples with a difference greater than zero to the upper-envelope set. This step allows to better follow the shape of the original data;
- Impute the updated upper-envelope set by means of PCHIP;
- Remove the two previous and two later months from NDI_{tr}.

The definition of NDI_{tr} allows to better model the beginning and the end of the SITS, thus smoothing discontinuities and possible errors in LCCD analysis.

2.4 Land Cover Change Detection

A limited number of methods have been developed in the literature that allow the analysis of long SITS for Change Detection (CD) applications. Most of state-of-the-art methods: (1) have been developed for medium and/or low spatial resolution applications; (2) make use of a single spectral value per each evaluated year; and (3) focus on single LC only (e.g., forest and/or vegetation). In order to map the changes in this paper, the Breaks For Additive Seasonal and Trend (BFAST)[15] is considered because of its wide use in literature and its capacity of being scalable to different spatial resolutions, other than the ones for which it was originally developed.

BFAST is a generic CD approach for SITS, involving the detection and characterization of BFAST. BFAST integrates the iterative decomposition of SITS into trend, seasonal and noise components with methods for detecting changes, without the need to select a reference period, set a threshold, or define a change trajectory. The main limitation of this method is that it has been developed for MODIS data and tested mainly on NDVI, and a few vegetation indices, and in particular for forest change detection. In this paper, we apply the BFAST to all the F features in order to increase the capability of detecting changes other than vegetation related ones. The final product is an image with two channels, one corresponding to the years in which a change has happened (varying from 0-5, with 0 = No-Change), and another providing information about the probability of a given change to have happened. The accuracy of the detection, is highly dependent on the SITS fitting quality, as well as the features and the speed of the change over the years.

3. STUDY AREAS AND PRE-PROCESSING

The proposed approach was applied to a 5 year Landsat 5, 7 and 8 SITS and over two different study areas. The acquisition period is the same for both datasets, being January 1st 2013 – December 31st 2017. The two areas are located in quiet different parts of the world (see Figure 2 and Figure 3):

- Dataset 1: located in the West-Central Amazonian rainforest area of Brazil. Here, a hydroelectric plant has been built in 2017, where it is easy to see that a huge area has been flooded. This location allows us to analyze the class change from forest to water;
- Dataset 2: located in the North-West desert of Saudi Arabia. Here, several central pivot crops have been built and can be easily identified in recent years, in particular between 2015 and 2017. In this case, changes happened along different periods, and are mostly related to desert becoming central pivot cropland class.

The size of datasets 1 and 2 is of $4km \times 4km$ ($133px \times 133px$). Data were downloaded directly from GEE[16], where the USGS Landsat Surface Reflectance Tier 1 is available. This particular collection includes atmospherically corrected surface reflectance from the Landsat 5 ETM, Landsat 7 ETM+ and Landsat 8 OLI/TIRS sensors. For Landsat 5 and 7 data have been atmospherically corrected using LEDAPS, whereas for Landsat 8, data have been atmospherically corrected using LaSRC. All datasets include a cloud, shadow, water and snow mask produced using CFMASK, as well as a per-pixel saturation mask.

Given the use of different atmospheric correction methods among Landsat 5-7 and Landsat 8 sensors, a further homogenization was carried out between the two in order to render the feature extraction process fully comparable in time.

The method proposed by Roy *et al.*[17] was followed. Additional to this correction, a cloud mask condition was imposed in order to avoid adding both highly cloudy images (cloud coverage higher than 70%) and cloudy pixels in any time series.

Finally, feature extraction was carried out (Section 2) and data downloaded to proceed with further steps. The time required to extract each feature and download the respective data, highly depends on the amount of data (number of images and/or free cloud pixels) per year. The average time, per feature, for dataset 1 was of 20 minutes, whereas for dataset 2 was of 30 minutes. The total number of images available per study area and dataset is shown in Table 1, where it is clear how for dataset 1, there are less images than for dataset 2. This being related to the climate characteristics of both areas. The Amazon region (dataset 1) is notoriously humid, with rainfall generally more than $2000mm$ per year and reaching as high as $3000mm$ in parts of the western Amazon. For Saudi Arabia, annual rainfall is extremely low. The Asir region (South-West) differs in that it is influenced by the Indian Ocean monsoons, when an average of $300mm$ of rainfall occurs, which is about 60 percent of the annual precipitation.

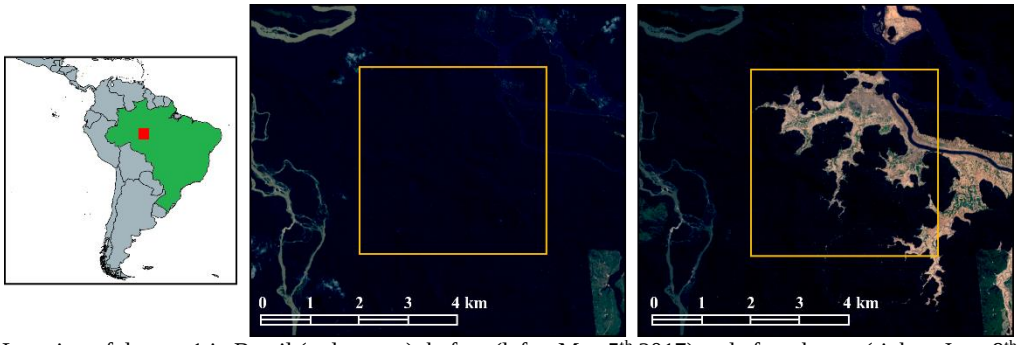

Figure 2. Location of dataset 1 in Brazil (red square): before (left – May 5th 2017) and after change (right – June 9th 2017) true color image example.

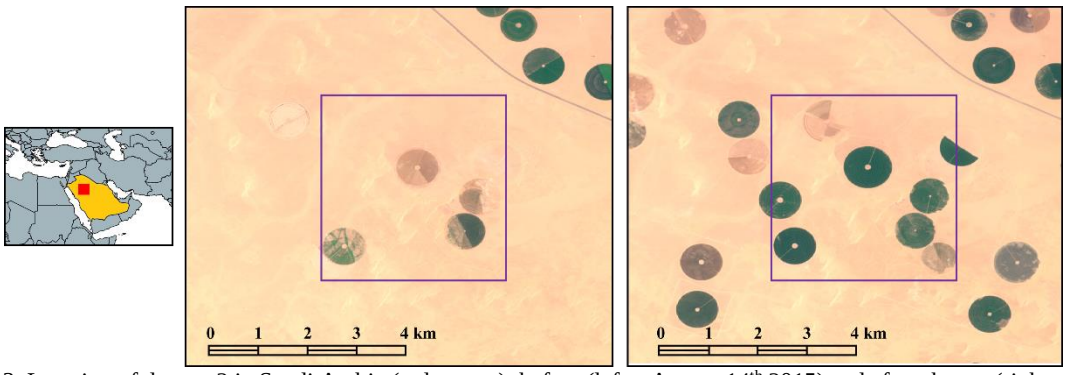

Figure 3. Location of dataset 2 in Saudi Arabia (red square): before (left – August 14th 2015) and after change (right – May 5th 2017) true color image example.

Table 1. Number of remaining images per year and per dataset after cloud coverage filtering (>70%).

Year	Dataset 1	Dataset 2
2013	27	69
2014	32	82
2015	36	90
2016	34	89
2017	31	87
TOTAL	160	417

4. EXPERIMENTAL RESULTS AND DISCUSSION

In order to evaluate the proposed approach, three types of analysis were carried out: (i) comparison of the fitting SITS stage with other state of the art methods (i.e., Cubic Splines and Univariate Splines filters). The selection of Cubic Splines and Univariate Splines methods is related to: i) their easier adaptation to irregularly acquired SITS, ii) their independence from harmonic or cyclic behaviors and; iii) their low computational time (when compared to other methods in literature[13]).

It is worth noting that the computational time of these two fitting methods and the proposed one are rather low (few seconds per feature) and comparable among each other. (ii) evaluation of the fitting process by means of the Mean Square Error (MSE) in comparison with original acquisitions and over different years and NDIs and; iii) change detection evaluation with BFAST for the three fitting methods.

4.1 Feature Extraction

The different Landsat sensors contain a total of 6 common spectral bands, being: Red, Blue, Green, NIR, SWIR1 and SWIR2. Following equation (2), that gives us a total of 15 possible NDIs. Nevertheless, it has already been demonstrated in literature that combinations of the different spectral bands can result in redundant information. In order to reduce the number of features, a Multiscale Superpixelwise Kernel Principal Component Analysis (MSK-PCA)[18] was used, resulting in a total of 8 features (see Table 2 for details, where NDI_8 = NDVI).

Table 2. Reduced set of NDI_f features.

NDI_f	B_i	B_j
1	Blue	SWIR2
2	Blue	Red
3	Green	SWIR1
4	Blue	SWIR1
5	NIR	SWIR2
6	Red	SWIR1
7	Red	SWIR2
8	NIR	Red

4.2 Time Series Regularization

The proposed SITS regularization method was compared to the state of the art ones: Cubic Splines and Univariate Splines (see Figure 4 and Figure 5). To better understand the correct regularization of data, the original acquisitions, in a linear reconstruction, were used for both qualitative and quantitative analysis. Given the big amount of features, analyzed years and extension of the area, only examples of reconstruction for a non-vegetation and one vegetation pixel (in three different features) are shown for Dataset 1 (as an example). Finally, in order to improve visualization, NDIs original range has been rescaled from $[-1, 1]$ to $[-100, 100]$.

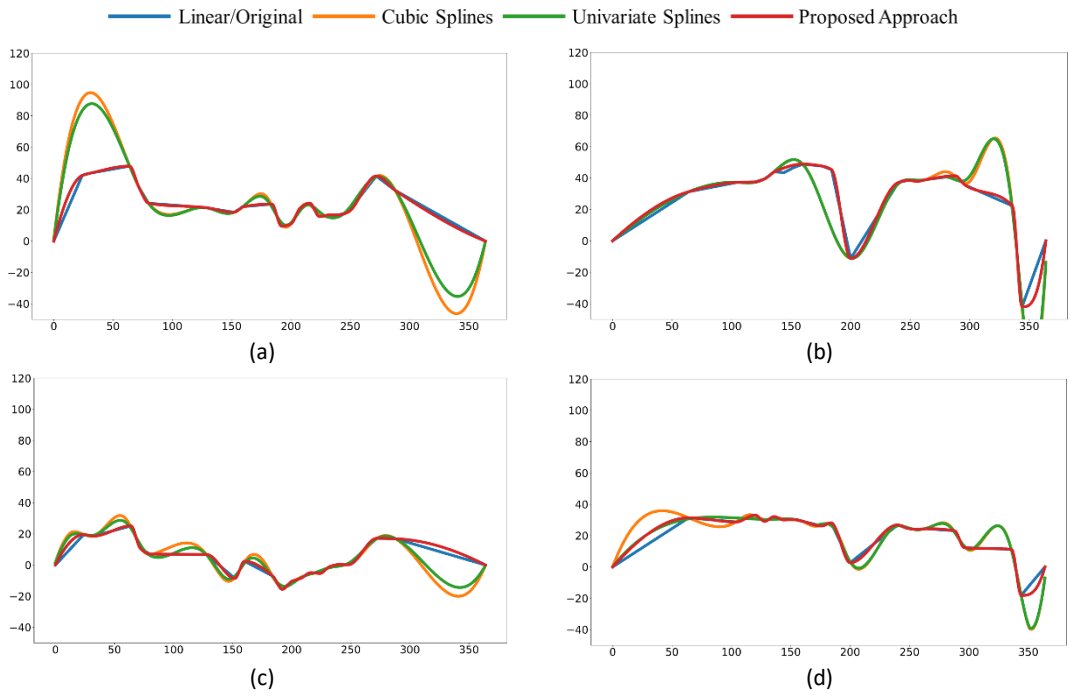

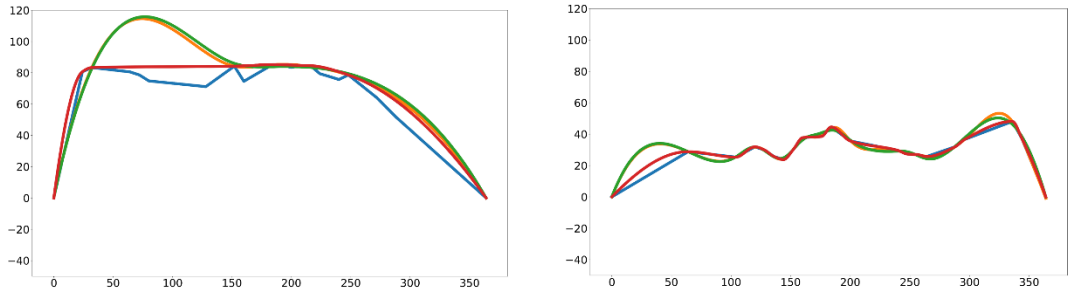

Figure 4. SITS fitting reconstruction for a non-vegetation pixel in Dataset 1. Left column corresponds to year 2016, whereas right column corresponds to year 2017. (a) and (b) NDI_1; (c) and (d) NDI_2; and (e) and (f) NDI_8 (NDVI).

Figure 4.a and b, for NDI1 clearly show how the proposed strategy for building NDI_{tr} helps to ensure the correct modelling of beginning and end of SITS trend in time. The same situation happens for a vegetation pixel, where in Figure 5.a and c the trend for the two state of the art methods diverges from the original acquisitions. Such behavior can result in the generation of fake changes over time. Another important finding is the fact that state of the art methods not only fail at properly following the original trend, but also at respecting the range in which the values must move (Figure 4.e). As a consequence, values are higher than 100 and sometimes also lower than -100.

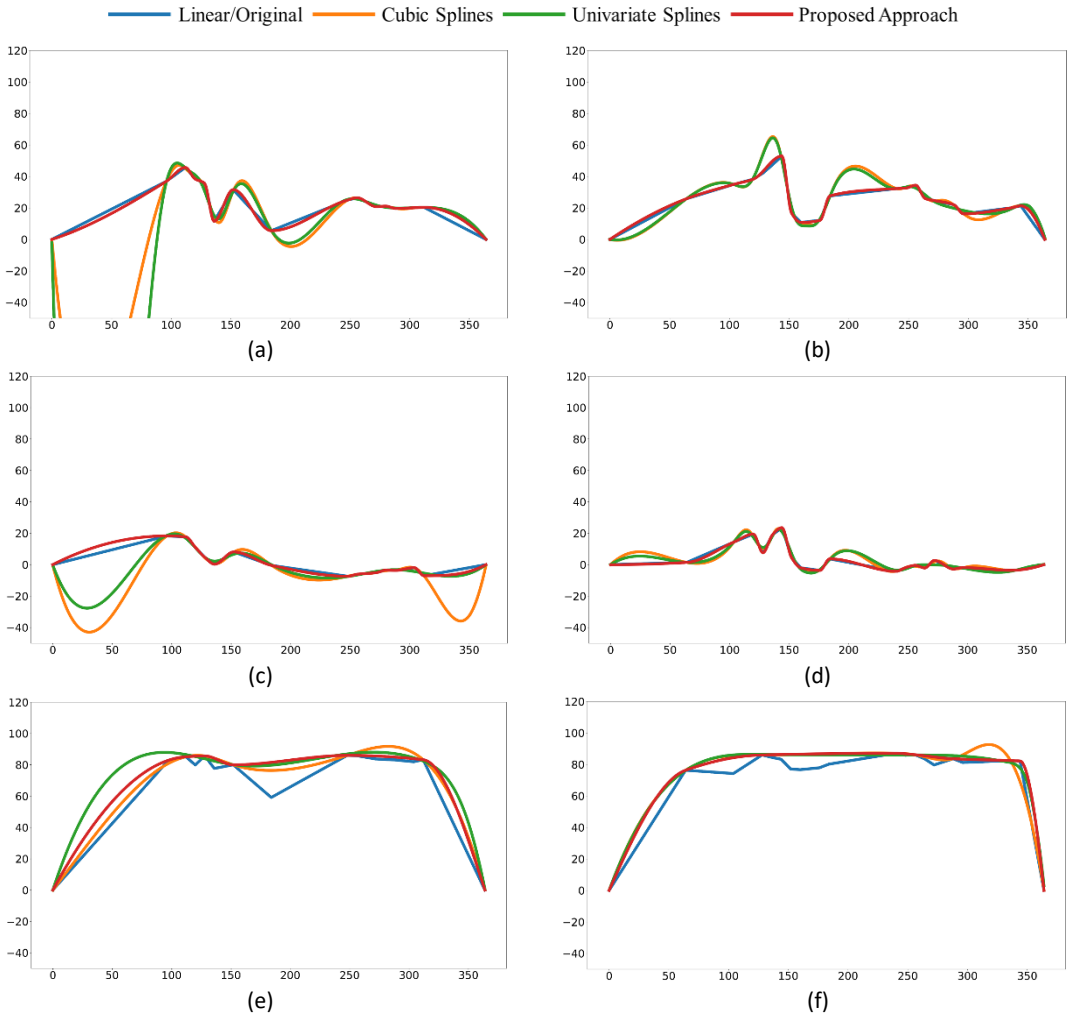

Figure 5. SITS fitting reconstruction for a vegetation pixel in Dataset 1. Left column corresponds to year 2014, whereas right column corresponds to year 2017. (a) and (b) NDI_1; (c) and (d) NDI_2; and (e) and (f) NDI_8 (NDVI).

It is important to recall that the previous analysis is performed at year level, therefore, MSE analysis is performed also at single year level. In this case, mean MSE for all the pixels in each of the datasets, for all the features and all the years are presented in Table 3 and Table 4. Looking at the results, it is clear that the proposed approach outperforms the two methods from literature in all the NDI_f. One particular case happens for Dataset 1 in 2015, where error for state of the art methods is quiet high, compared to the other years.

Table 3. Mean MSE for Dataset 1 and for the three methods: (1) Cubic Splines, (2) Univariate Splines and; (3) Proposed approach. Values are provided in 100, as per the NDI_f features range.

Year	Method	NDI_1	NDI_2	NDI_3	NDI_4	NDI_5	NDI_6	NDI_7	NDVI
2013	1	14.4685	13.4266	5.8580	3.7791	6.7120	2.3665	12.9173	1.2139
	2	13.4626	11.9403	5.6214	3.5098	6.4501	2.0988	11.5676	1.1986
	3	0.1650	0.0301	0.3587	0.5175	0.5082	0.5505	0.1424	0.5590
2014	1	28.2215	17.3653	6.8051	7.0089	5.8453	3.8689	16.6811	1.4317
	2	27.1755	15.3563	6.7078	6.8967	5.2785	3.3022	15.7659	1.2423
	3	0.3837	0.0370	0.4185	0.8486	0.5412	0.6428	0.1486	0.6957
2015	1	22.5663	34.6738	27.4440	20.3371	9.3072	21.2538	17.0213	26.1367
	2	16.6380	20.2583	27.1023	19.4769	9.0056	20.5540	16.6788	22.5196
	3	0.1025	0.0175	0.5770	0.5729	1.0607	0.6492	0.1236	0.9527
2016	1	3.3499	2.4605	3.8010	3.8009	1.9005	5.2196	2.2799	3.9081
	2	3.9482	2.4723	3.7621	3.6558	1.8760	5.8789	2.2509	4.2872
	3	0.0797	0.0176	0.3768	0.6396	0.1907	0.6560	0.0333	0.5295
2017	1	4.9110	1.7049	5.8294	5.0903	1.4877	2.6801	2.5317	1.7881
	2	5.2731	2.1867	5.7698	4.9878	1.4566	2.6521	2.4675	1.7525
	3	0.1296	0.0248	0.2006	0.5610	0.1971	0.3839	0.0834	0.3778

Looking at the results for dataset 2 (Table 4), for year 2013 (where mainly desert class is in the area), the MSE for state of the art of all the features is quiet high. Whereas, as we move toward the years, and more and more central pivot crop fields appear in the area, the general error in all the features starts to reduce, especially for NDVI. This behavior is clear not only for the state of the art methods, but also for the proposed approach. This amount of error in the different features is expected to affect the final LCCD maps, where more false alarms might appear (in salt-pepper way) along the two datasets.

Table 4. Mean MSE for Dataset 2 and for the three methods: (1) Cubic Splines, (2) Univariate Splines and; (3) Proposed approach. Values are provided in 100, as per the NDI_f features range.

Year	Method	NDI_1	NDI_2	NDI_3	NDI_4	NDI_5	NDI_6	NDI_7	NDVI
2013	1	7.6973	12.2664	10.4796	7.3862	4.2228	4.7144	4.4502	30.6330
	2	8.1290	15.7432	11.1450	8.8090	4.5677	4.9801	5.1154	32.4534
	3	0.6373	0.3459	0.2196	0.6995	0.0105	0.0659	0.0357	3.4913
2014	1	5.3238	2.2826	0.2930	2.2987	0.2720	0.1646	0.1991	0.3631
	2	2.9180	2.5970	0.3124	2.2745	0.2341	0.1621	0.1876	0.3532
	3	0.0558	0.0185	0.0165	0.0665	0.0052	0.0077	0.0034	0.0132
2015	1	3.3039	1.3314	0.1449	2.7849	0.2112	0.0916	0.1105	0.2658
	2	2.0849	1.0825	0.1176	2.6566	0.2018	0.1102	0.9807	0.2480
	3	0.0613	0.0136	0.0033	0.0861	0.0059	0.0016	0.0018	0.0092
2016	1	3.3124	0.7256	0.1967	2.4430	0.6734	0.3355	0.1799	1.1079
	2	2.1027	2.1318	0.1821	2.3440	0.5567	0.3276	0.1765	1.0893
	3	0.0683	0.0164	0.0070	0.0871	0.0083	0.0059	0.0027	0.0497
2017	1	2.4121	1.0009	0.9639	2.0035	2.0087	1.0141	0.1799	1.9517
	2	8.2824	5.9994	0.9501	1.9801	1.9945	1.0023	0.1607	2.0676
	3	0.0585	0.0158	0.0093	0.0935	0.0161	0.0170	0.0027	0.1282

4.3 Change Detection

Based on the results achieved in previous step and because of space constrains, LCCD results are only shown for a single feature. In this case, NDVI (NDI_8) feature was selected, but results are similar and qualitatively good in different features, and able to detect different types of changes, according to the feature. Figure 6 and Figure 7 show the CD results for the two datasets with NDVI feature and the three compared methods. A false color composition image of the changes has been also added for comparison. Even though the false color composition only represents one moment in time of the whole SITS, it is possible to understand the main changes occurred in each area. It is also clear how the proposed approach

outperforms the state of the art ones, in particular for the dataset 1, where mainly vegetation classes are present (the most complex ones), but the BFAST combined with the state of art reconstruction methods, fails at properly identifying any change.

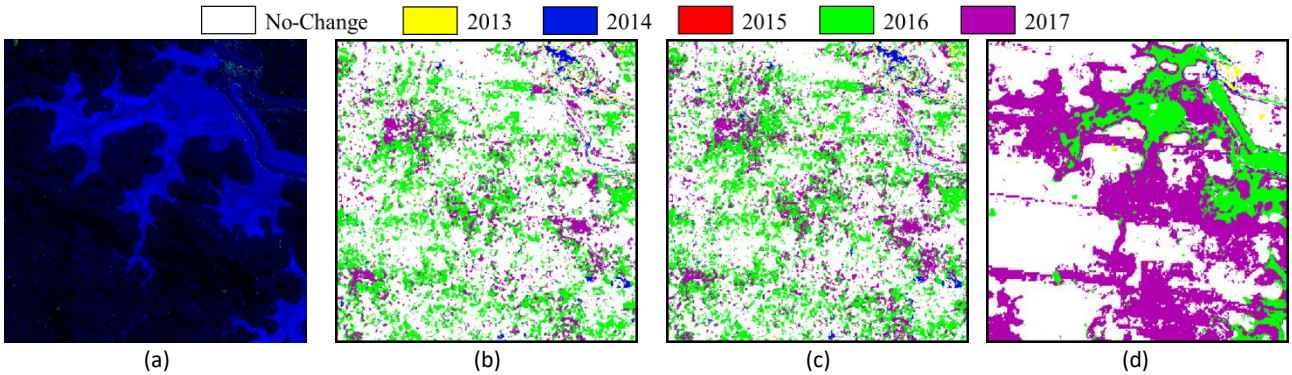

Figure 6. (a) RGB false color composition of Dataset 1, R: Red at time 1, G: Green at time 2 and B: Blue at time 1. LCCD maps in the period 2013-2018 for NDVI feature with (b) Cubic Splines, (c) Univariate Splines and (d) Proposed Approach.

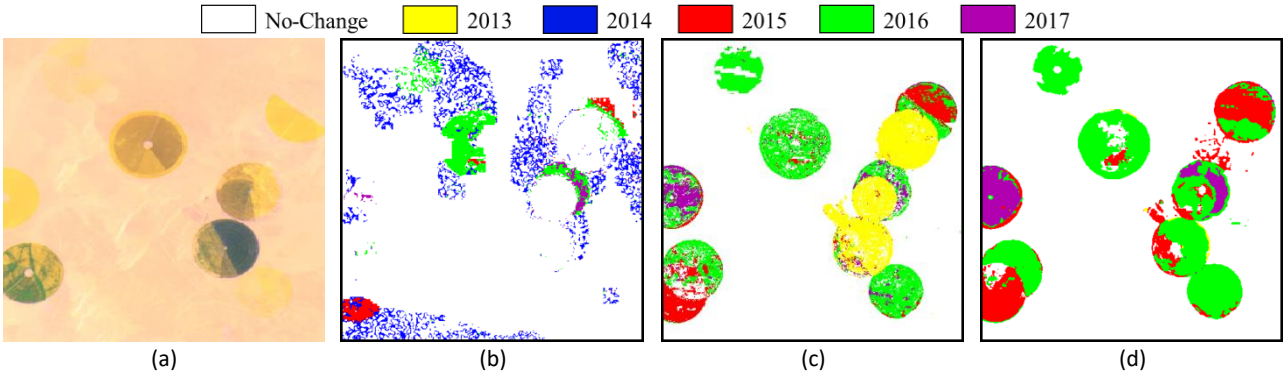

Figure 7. (a) RGB false color composition of Dataset 2, R: Red at time 1, G: Green at time 2 and B: Blue at time 1. LCCD maps in the period 2013-2018 for NDVI feature with (b) Cubic Splines, (c) Univariate Splines and (d) Proposed Approach.

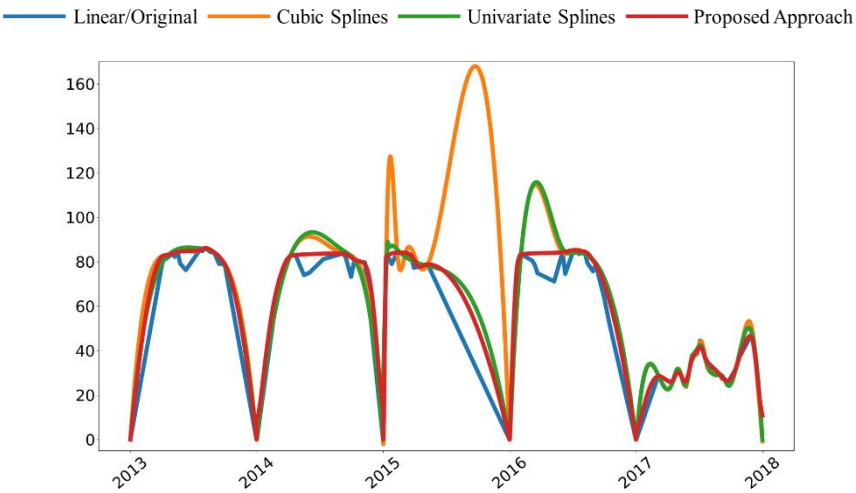

Figure 8. SITS-NDVI fitting reconstruction for a vegetation to non-vegetation pixel in Dataset 1 in the period 2013-2017.

To further understand the reasons why state of the art methods fail at providing proper information for an accurate CD, a SITS plot for NDVI feature over the period 2013-2017 for both datasets has been plot (see Figure 8 and Figure 9). In Figure 8, a pixel that changes from vegetation to non-vegetation is shown. This change happens during 2017, nevertheless,

both state of the art methods show a peak during 2015 and 2016, different from the standard trend of the previous years. Such peaks result in BFAST detecting them as changes, whereas no real change has occurred in the period. In Figure 9, a pixel that changes from non-vegetation to vegetation is shown. In this case, the state of the art methods and proposed approach have a similar behavior in the 2013-2016 period, which means that changes will be modeled in the proper way. Nevertheless, looking at year 2017, it is clear that magnitude of change increases much more for the state of the art methods (actually overpassing the 100 range). Which can result in a different interpretation of results. Overall, the proposed approach for SITS fitting allows to better model the features trend over time, resulting in a better detection of changes in the corresponding year and at a similar magnitude to that of real acquisitions.

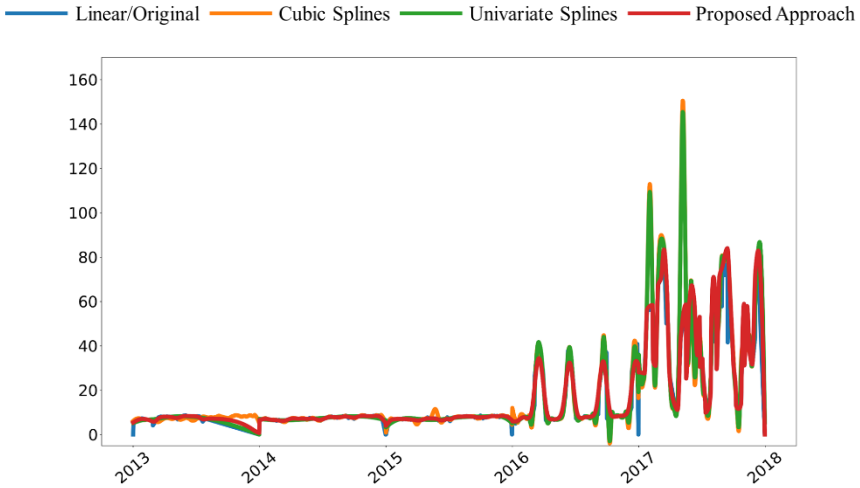

Figure 9. SITS-NDVI fitting reconstruction for a non-vegetation to vegetation pixel in Dataset 2 in the period 2013-2017.

It is important to note that in order to produce a more accurate LCCD map, that takes into account information from the eight features, a LC map (if available) can be used in order to provide information on the type of change that has happened.

5. CONCLUSION AND FUTURE DEVELOPMENTS

An approach for SITS fitting in the context of change detection has been presented. The approach is fully automatic and applicable to any high spatial resolution sensor. The approach presents an upper-envelope dropout strategy that is suitable for any NDI feature and any LC class. If available, it can exploit the LC information in order to further improve the reconstruction of SITS corresponding to vegetation classes. Compared to other standard fitting approaches, it better follows the real behavior of the original data, while at the same time reducing the noisy trend of data in time due to atmospheric conditions along acquisitions. Computational time is also low and comparable to that of literature methods. When the proposed approach is applied to a CD context, the detection of changes is improved by the fact that false changes are not introduced in the full reconstruction of the SITS.

As future developments, a method that allows to identify the type of change, as well as the duration of the change, is to be introduced. Though this strategy would require a supervised approach for the correct identification of the LC classes, it will allow to provide additional information relevant for CC analysis.

ACKNOWLEDGEMENT

This research has been partially developed under the project “High-Resolution Landcover - Climate Change Initiative + (CCI+)” funded by ESA.

REFERENCES

[1] Bovolo, F., Bruzzone, L. and Solano-Correa, Y. T., “Multitemporal Analysis of Remotely Sensed Image Data,” [Comprehensive Remote Sensing], S. Liang, Ed., Elsevier, Oxford, 156–185 (2018).

[2] Bradley, B. A., Jacob, R. W., Hermance, J. F. and Mustard, J. F., “A curve fitting procedure to derive inter-annual phenologies from time series of noisy satellite NDVI data,” Remote Sensing of Environment **106**(2), 137–145 (2007).

[3] Atkinson, P. M., Jeganathan, C., Dash, J. and Atzberger, C., "Inter-comparison of four models for smoothing satellite sensor time-series data to estimate vegetation phenology," Remote Sensing of Environment **123**, 400–417 (2012).
[4] Pouliot, D. and Latifovic, R., "Reconstruction of Landsat time series in the presence of irregular and sparse observations: Development and assessment in north-eastern Alberta, Canada," Remote Sensing of Environment **204**, 979–996 (2018).
[5] Zhou, J., Jia, L. and Menenti, M., "Reconstruction of global MODIS NDVI time series: Performance of Harmonic ANalysis of Time Series (HANTS)," Remote Sensing of Environment **163**, 217–228 (2015).
[6] Gerber, F., de Jong, R., Schaepman, M. E., Schaepman-Strub, G. and Furrer, R., "Predicting Missing Values in Spatio-Temporal Remote Sensing Data," IEEE Transactions on Geoscience and Remote Sensing **56**(5), 2841–2853 (2018).
[7] Savitzky, Abraham. and Golay, M. J. E., "Smoothing and Differentiation of Data by Simplified Least Squares Procedures.," Anal. Chem. **36**(8), 1627–1639 (1964).
[8] Zhao, K., Wulder, M. A., Hu, T., Bright, R., Wu, Q., Qin, H., Li, Y., Toman, E., Mallick, B., Zhang, X. and Brown, M., "Detecting change-point, trend, and seasonality in satellite time series data to track abrupt changes and nonlinear dynamics: A Bayesian ensemble algorithm," Remote Sensing of Environment **232**, 111181 (2019).
[9] Hermosilla, T., Wulder, M. A., White, J. C., Coops, N. C. and Hobart, G. W., "An integrated Landsat time series protocol for change detection and generation of annual gap-free surface reflectance composites," Remote Sensing of Environment **158**, 220–234 (2015).
[10] Zhu, Z. and Woodcock, C. E., "Continuous change detection and classification of land cover using all available Landsat data," Remote Sensing of Environment **144**, 152–171 (2014).
[11] "Google Earth Engine.", <https://earthengine.google.com/> (25 August 2020).
[12] Eklundh, L. and Jönsson, P., "TIMESAT for Processing Time-Series Data from Satellite Sensors for Land Surface Monitoring," [Multitemporal Remote Sensing], Y. Ban, Ed., Springer International Publishing, 177–194 (2016).
[13] Solano-Correa, Y. T., Bovolo, F., Bruzzone, L. and Fernández-Prieto, D., "A Method for the Analysis of Small Crop Fields in Sentinel-2 Dense Time Series," IEEE Transactions on Geoscience and Remote Sensing **58**(3), 2150–2164 (2020).
[14] Solano-Correa, Y. T., Bovolo, F., Bruzzone, L. and Fernández-Prieto, D., "Automatic Derivation of Cropland Phenological Parameters by Adaptive Non-Parametric Regression of Sentinel-2 NDVI Time Series," IGARSS 2018, 1946–1949 (2018).
[15] Verbesselt, J., Hyndman, R., Newnham, G. and Culvenor, D., "Detecting trend and seasonal changes in satellite image time series," Remote Sensing of Environment **114**(1), 106–115 (2010).
[16] "Landsat Collections in Earth Engine | Earth Engine Data Catalog.", Google Developers, <https://developers.google.com/earth-engine/datasets/catalog/landsat> (24 August 2020).
[17] Roy, D. P., Kovalskyy, V., Zhang, H. K., Vermote, E. F., Yan, L., Kumar, S. S. and Egorov, A., "Characterization of Landsat-7 to Landsat-8 reflective wavelength and normalized difference vegetation index continuity," Remote Sensing of Environment **185**, 57–70 (2016).
[18] Zhang, L., Su, H. and Shen, J., "Hyperspectral Dimensionality Reduction Based on Multiscale Superpixelwise Kernel Principal Component Analysis," 10, Remote Sensing **11**(10), 1219 (2019).